

Simulation of surface flows on a droplet in an oscillating pressure field

Tadashi Watanabe

Abstract—The surface flows on a droplet in an oscillating pressure field are simulated numerically by solving the Navier-Stokes equations using the Arbitrary Lagrangian-Eulerian and level set coupled method. Detailed transient flow fields in and around the droplet are calculated by performing parallel computations, and the flow phenomena in a thin layer around the droplet surface are discussed. The recirculation flow region is found to be formed at the top and bottom stagnation points on the droplet surface. It is also found that the oscillating flow with a phase shift appears in the thin layer along the droplet surface.

Keywords—Surface flow, Droplet, Oscillating pressure, Arbitrary Lagrangian-Eulerian method, Level set method.

I. INTRODUCTION

A levitated liquid droplet is used to measure material properties of molten metal at high temperature, since the levitated droplet is not in contact with a container, and the effect of container wall is eliminated for precise measurement [1]. The levitation of liquid droplet, which is also used for container-less processing of material, is controlled by using electromagnetic [2] electrostatic [3], or ultrasonic force [4] in the vertical direction. The levitated droplet is affected by an oscillating pressure field when the ultrasonic or acoustic levitator is used. Additionally, rotation is sometimes imposed on the droplet to stabilize its motion. The rotational motion is controlled by acoustic forces perpendicular to the vertical axis. It is thus important to know the behavior of droplet in an oscillating flow field. The streaming flows associated with ultrasonic levitator have been studied experimentally [5,6] and theoretically [7]. Although steady-state flows in and around the droplet were studied, transient flow fields or growth of the streaming flows have not yet been discussed well.

The flow field in and around the droplet in an acoustic standing wave is simulated numerically in this study. The droplet is assumed to be levitated in the centre of the simulation region, and the standing wave field is modelled with an oscillating boundary conditions. The flow field in and around the droplet is calculated using the arbitrary Lagrangian-Eulerian (ALE) method, where the

computational grid points for flow field are moved with the oscillating boundary velocity. The two-phase flow field is obtained using the level set method. In the level set method, the level set function, which is the distance function from the two-phase interface, is calculated by solving the transport equation using the local flow velocity. Incompressible Navier-Stokes equations are solved to obtain the flow field, and the effect of compressibility is taken into account as the density perturbation. The simulation program is parallelized by the domain decomposition technique using the Message Passing Interface (MPI) library, and parallel calculations are performed using a massively parallel computer system. The pressure field in and around the droplet is shown to see the acoustic standing wave including a droplet. Transient flow field in and around the droplet is shown next, and characteristics of the oscillating flow field especially in the thin layer on the droplet surface are discussed.

II. NUMERICAL METHOD

A. Governing Equations

Governing equations for the droplet motion are the equation of continuity and the incompressible Navier-Stokes equation [8]:

$$\nabla \cdot \mathbf{u} = 0, \quad (1)$$

and

$$\rho \frac{D\mathbf{u}}{Dt} = -\nabla p + \nabla \cdot (2\mu\mathbf{D}) - \mathbf{F}_s \quad (2)$$

where ρ , \mathbf{u} , p and μ , respectively, are the density, the velocity, the pressure and the viscosity, \mathbf{D} is the viscous stress tensor, and \mathbf{F}_s is a body force due to the surface tension. External force fields such as the gravity are not simulated in this study. The surface tension force is given by

$$\mathbf{F}_s = \sigma\kappa\delta\nabla\phi \quad (3)$$

where σ , κ , δ and ϕ are the surface tension, the curvature of the interface, the Dirac delta function and the level set function, respectively. The level set function is a distance function defined as the normal distance from the interface: $\phi=0$ at the interface, $\phi<0$ in the liquid region, and $\phi>0$ in the gas region. The curvature of the interface is expressed in terms of ϕ .

Manuscript received June 12, 2011; Revised version received August 12, 2011. This work was supported in part by MEXT Grants-in-Aid for Scientific Research (c), No. 21560230.

Tadashi Watanabe is with the Center for computational Science and e-Systems, Japan Atomic Energy Agency, Tokai-mura, Naka-gun, Ibaraki-ken, 319-1195, JAPAN(phone: 81-29-282-5029; fax: 81-29-282-6728; e-mail: watanabe.tadashi66@jaea.go.jp).

$$\kappa = \nabla \cdot \left(\frac{\nabla \phi}{|\nabla \phi|} \right) \quad (4)$$

The density and viscosity are, respectively, given by

$$\rho = \rho_l + (\rho_g - \rho_l)H \quad (5)$$

and

$$\mu = \mu_l + (\mu_g - \mu_l)H \quad (6)$$

where the subscripts g and l indicate gas and liquid phases, respectively. In Eqs. (5) and (6), H is the Heaviside-like function defined by

$$H = \begin{cases} 0 & (\phi < -\varepsilon) \\ \frac{1}{2} \left[1 + \frac{\phi}{\varepsilon} + \frac{1}{\pi} \sin\left(\frac{\pi\phi}{\varepsilon}\right) \right] & (-\varepsilon \leq \phi \leq \varepsilon) \\ 1 & (\varepsilon < \phi) \end{cases}, \quad (7)$$

where ε is a small positive constant for which $|\nabla \phi| = 1$ for $|\phi| \leq \varepsilon$. The evolution of ϕ is given by

$$\frac{D\phi}{Dt} = 0 \quad (8)$$

In this study, the ALE method [9] is applied, and the computational grid is moved with the same velocity as the velocity of the boundary condition. The substantial derivative terms in Eqs. (2) and (8) are thus defined by

$$\frac{D}{Dt} = \frac{\partial}{\partial t} + (u - U) \cdot \nabla \quad (9)$$

In order to maintain the level set function as a distance function, reinitialization of the level set function is proposed by solving the following equation [8]:

$$\frac{\partial \phi}{\partial \tau} = \text{sign}(\phi_0)(1 - |\nabla \phi|) \quad (10)$$

where τ is an artificial time, and $\text{sign}(\phi_0)$ indicates the sign of the level set function at the beginning of the reinitialization procedure. The level set function becomes a distance function in the steady-state solution of Eq. (10). The smoothed sign function proposed for numerical treatment of reinitialization [14] is used for Eq. (10);

$$\text{sign}(\phi) = \frac{\phi}{\sqrt{\phi^2 + h^2}}, \quad (11)$$

where h is the spatial increment in the finite difference method for solving the governing equations. A smoothed version of the sign function was also used in [8].

The following equation is also solved to preserve the total mass in time [10];

$$\frac{\partial \phi}{\partial \tau} = (A_0 - A)(P - \kappa) |\nabla \phi| \quad (12)$$

where A_0 denotes the total mass for the initial condition and A denotes the total mass corresponding to the level set function. P is a positive constant for stabilization, and 1.0 was used in [10]. The total mass is conserved in the steady-state solution of the above equation. The effects of Eqs. (10) and (12) have been discussed in [15].

The effect of compressibility is taken into account simply as the density perturbation, since the amplitude of pressure variation and thus the density variation are both small in this study. The density perturbation is defined by

$$\delta \rho = \delta p / c^2 \quad (13)$$

where, c is the sound speed.

The finite difference method is used to solve the governing equations. The staggered mesh is used for spatial discretization of velocities. The convection terms are discretized using the second order upwind scheme and other terms by the second order central difference scheme. Time integration is performed by the second order Adams-Bashforth method. The SMAC method is used to obtain pressure and velocities [12]. The pressure Poisson equation is solved using the Bi-CGSTAB method. The domain decomposition technique is applied and the MPI library is used for parallel computations, and the block Jacobi preconditioner is used for the parallel Bi-CGSTAB method [11,13].

B. Problem Description

The flow field in and around the droplet in an oscillating pressure field is simulated in the following. The oscillating pressure field is modelled with the oscillating boundary conditions, and the droplet is assumed to be levitated in the centre of the simulation region. In order to simulate detailed flow field in the thin layer on the droplet surface, the calculation grid size is very small in this study. A large number of calculation grid points are thus necessary, and the calculation time becomes very long. The simulation program is thus parallelized by the domain decomposition method in the vertical direction of the simulation region using the message passing interface (MPI) library, and parallel calculations using 256 processors of Fujitsu PRIMERGY BX900 parallel computer system is used.

The simulation region is a two-dimensional rectangular region shown in Fig. 1. Vertical and horizontal sizes of the simulation region are 6.4 mm and 3.2 mm, respectively, and the radius of the droplet is 2 mm. A half the droplet is simulated as shown in Fig. 1. Water and air densities and viscosities are assumed for the inside and outside of the droplet, respectively. The slip and symmetric boundary conditions are applied at the right and left sides of the simulation region, respectively, and the oscillating velocity

conditions given by the following equation are used at the top and bottom boundaries:

$$U = A \omega \cos(\omega t) \quad (14)$$

where the oscillation amplitude A is 0.076 m and the angular frequency Ω is 1.26×10^5 rad/s. These values are almost corresponding to the sound pressure of 0.25 kPa and the sound frequency of 20 kHz in air. The sound speed is 340 m/s for air and 1400 m/s for water. The oscillation velocity given by Eq. (13) is also used as the grid velocity in Eq. (9) used in the ALE method. The number of calculation grid points is 1000 x 2000, and the grid size is 3.2 μm both in horizontal and vertical directions. The time step size is set equal to 0.08 μs , and 625 time steps are corresponding to one oscillation period of the pressure field.

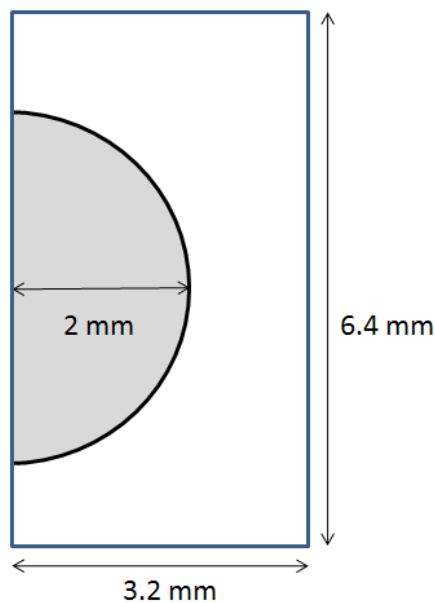


Fig. 1 Schematic of droplet and a simulation region.

III. RESULTS AND DISCUSSION

A. Parallel Calculation

The simulation program is parallelized by the domain decomposition method using the MPI library, and parallel calculations using 256 processors are performed. In Fig. 2, the parallel performance is shown for the present simulations as a speedup of calculations.

The total calculation time is indicated as Elapse Time, and the time for matrix calculation is shown as Matrix Time. The number of time steps is five, and I/O process is included in Fig. 2. The CPU time using single processor is 3345.6 s for Elapse Time and 3316.8 s for Matrix Time. The time for matrix calculation is thus more than 99 % of the total calculation time in this study. The number of iterations for the Bi-CGSTAB method is different in each time step and varied from 668 to 1883 for the single processor case. The speedup or parallel performance is not good

as shown in Fig. 2. About 77 times speedup is achieved for matrix calculations using 256 processors. The number of iterations is increased as the number of processors increases. The number of iterations for the 256 processor case is varied from 1459 to 9387. The time for data communication, thus, becomes large as well as the calculation time, as the number of processors increases. Actual calculation time for 625 time steps using 256 processors is about 4300 s. This calculation time depends on the convergence of the Bi-CGSTAB method, and 10^{-6} is used as the convergence criterion for the relative errors in the following simulations. By considering the cache effect, which depends on the data size, the parallel performance could be improved and better than that shown in Fig. 2.

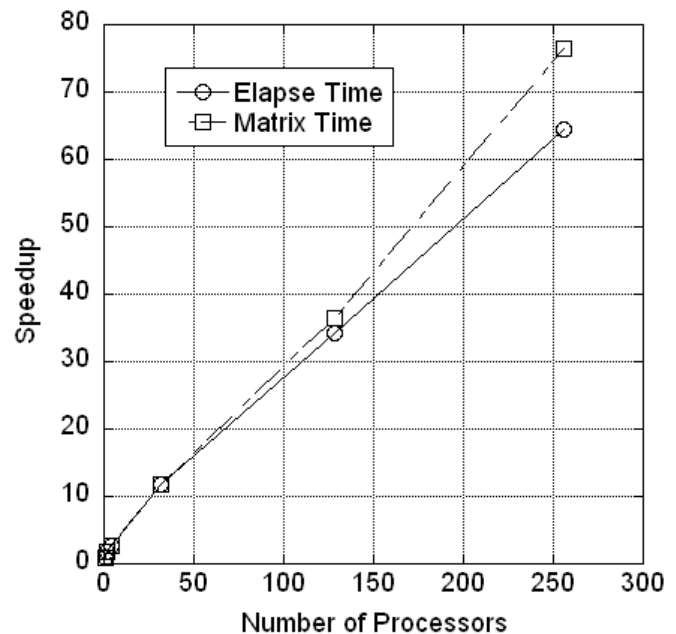


Fig. 2. Speedup of parallel calculations.

B. Oscillating Pressure Field

The simulated pressure field is shown in Figs. 3 and 4. The vertical pressure distributions along the right side of the simulation region are shown in Fig. 3, where the pressure variation at 155, 305, 460, and 625 time steps are shown without the droplet. One oscillation period is divided into 625 time steps in our simulations, and thus, the pressure variations at about 1/4, 2/4, 3/4, and 4/4 period of one oscillation are shown in Figs. 3 and 4. At 155 time steps, the pressure variation is still very small. But at 305 time steps, the pressure variation is almost the maximum and decreases upward. The pressure variation is again very small at 460 time steps, and very large with increasing pressure at 625 time steps. It is found that the standing wave field with the pressure node at the center of the simulation region is simulated well by the present numerical method using the ALE and level set coupled method with a pseudo compressibility. In our simulations, the sound pressure of 0.25 kPa is assumed for the oscillation pressure field. The vertical simulation region is much smaller than the wave length, and thus the maximum pressure shown in Fig. 3 is

smaller than 0.25 kPa. The vertical pressure distributions along the center axis of the droplet are shown in Fig. 4. It is found that the pressure distribution is much affected by the droplet in comparison with the right side pressure shown in Fig. 3, especially at the top and bottom of the droplet surface. The pressure distribution is almost linear in the droplet region, since the sound speed is larger in the droplet comparing to the sound speed in air. The oscillating pressure field is thus shown to be simulated well through the droplet.

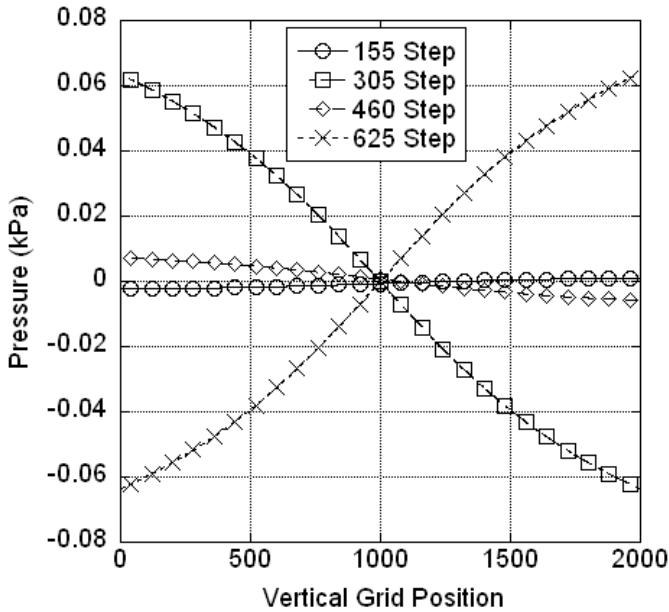


Fig. 3. Vertical pressure variation outside the droplet.

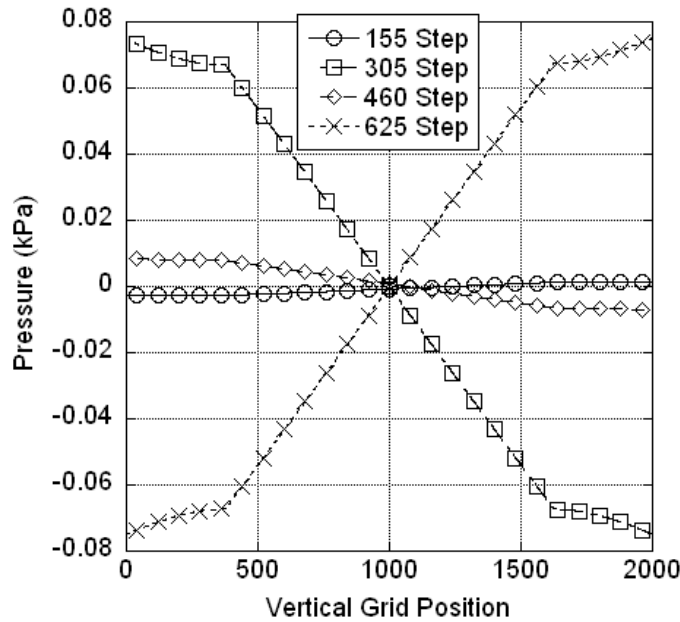


Fig. 4. Vertical pressure variation along the droplet centre.

C. Early Flow Field in and around the Droplet

Simulated flow fields in and around the droplet in the early

stage of transients are shown here. Overall flow fields in the first oscillation period are shown in Fig. 5. The velocity field is found to be formed corresponding to the pressure field shown in Fig. 3. The magnitude of the velocity is large at 155 and 460 time steps, and small at 305 and 625 time steps. The pressure gradient shown in Fig. 3 is, however, large at 305 and 625 time steps and small at 155 and 460 time steps. Downward flow field

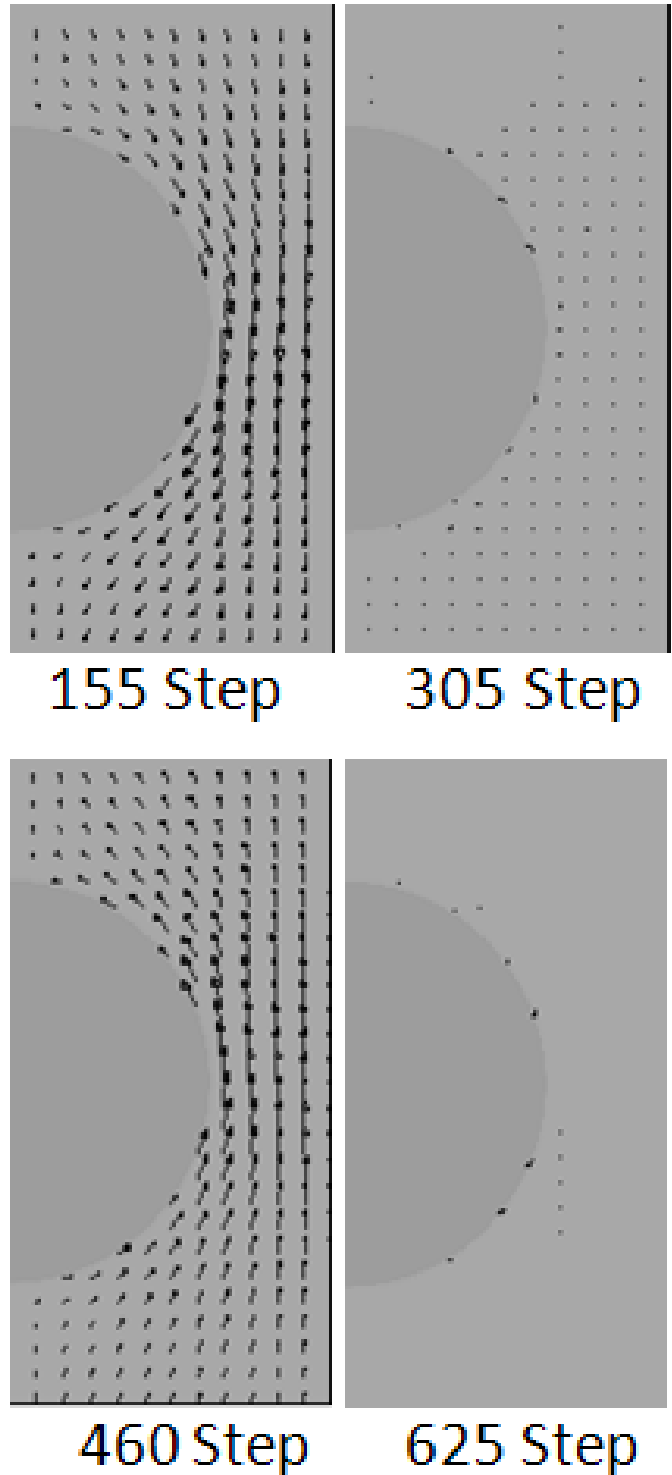


Fig. 5. Overall flow field around the droplet.

is clearly seen at 155 time steps and the upward flow field is seen at 460 time steps. These oscillating flow fields are formed

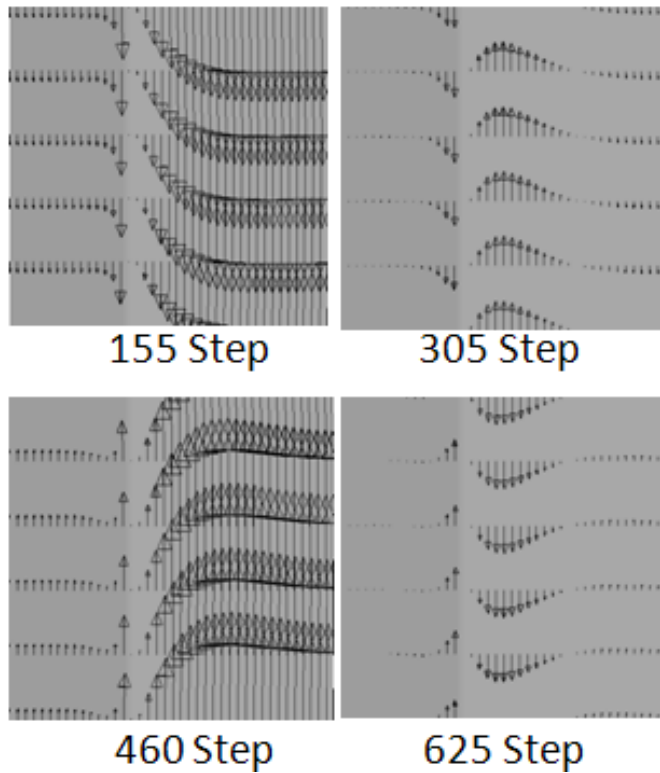


Fig. 6. Flow field at the side of the droplet.

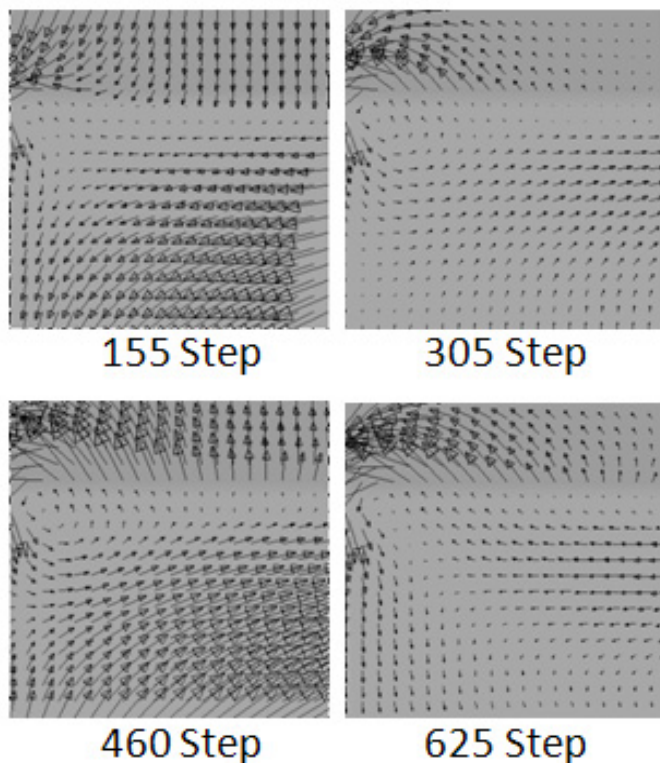


Fig. 7. Flow field at the bottom of the droplet.

again in the next oscillation period from 625 to 1250 time steps, and so on. It is noted that the flow field inside the droplet is calculated along with the outside flow field in the present numerical method, but the magnitude of inside velocity field is very small comparing to the outside velocity field, and thus it is not seen in Fig. 5.

The flow field at the side surface of the droplet is shown in Fig. 6, where the small region with several grid points is shown to see the surface layer clearly. The magnitude of the velocity vector inside the droplet, which is shown in the left part of Fig. 6, are 100 times larger than that outside the droplet, which is shown in the right part of Fig. 6. It is found at 155 time steps that the inside flow field is formed due to the outside downward flow field. At 305 time steps, the outside flow is upward near the droplet surface, while the outer flow away from the droplet is still downward and very small. It is also shown in Fig. 5 that the outside flow field or the outer flow away from the droplet is almost zero at 305 time steps. The outside flow field is clearly upward at 460 time steps, and the inside flow field seems to be dragged by the outside flow field again as was the case at 155 time steps. At 625 time steps, the outside flow is downward near the droplet surface, while the outer flow away from the droplet is still upward and very small. This flow field is almost the reversed flow field of that at 305 time steps.

The flow field at the bottom surface of the droplet is shown in Fig. 7, where the small region with several grid points is again shown. The left side of the flow field shown in Fig. 7 is the centre axis shown as the left side boundary in Figs. 1 and 5. The magnitude of the velocity vector inside the droplet, which is shown in the upper part of Fig. 7, are 10 times larger in this case than that outside the droplet, which is shown in the lower part of Fig. 7. It is found at 155 time steps that the outside flow is going from the right to the centre, and then downward. At 305 time steps, the outside flow is going from the centre to the right along the droplet surface, while the outer flow is very small. It is thus found that the upward flow near the droplet surface shown in Fig. 6 at 305 time steps is coming from the bottom of the droplet. A small vortex or recirculation flow region is found on the droplet surface, and the upward flow is formed by this vortex. The outside flow is clearly upward at 460 time steps, and is going from the centre to the right along the droplet surface. The small vortex on the droplet surface is seen again at this time step. At 625 time steps, the outside flow is from the right to the centre, while the outer flow is very small. The vortex is still seen, though it is small. A similar vortex or recirculation region also appears at the top of the droplet, though it is not shown here. It is found that the oscillating flow in the thin layer on the droplet surface with a slightly different oscillation phase is formed by the vortex or recirculation flow at the bottom and top of the droplet.

D. Later Flow Field in and around the Droplet

Overall flow fields in one oscillation period at later time are shown in Fig. 8. The flow fields are in the 25-th oscillation period from 15000 time steps to 15625 time steps. It is shown that the velocity fields are similar to those in Fig. 5 for the first

oscillation period from 0 to 625 time steps. The magnitude of the velocity is large at 15155 and 15460 time steps, and small at 15305 and 15625 time steps. Downward flow is seen at 15155 time steps and the upward flow is seen at 15460 time steps. The oscillating flow field is, thus, found to be established immediately in the 1st oscillation period and iterated in the following oscillation periods. The flow field inside the droplet is still very small comparing to the outside flow field, and it is again not seen

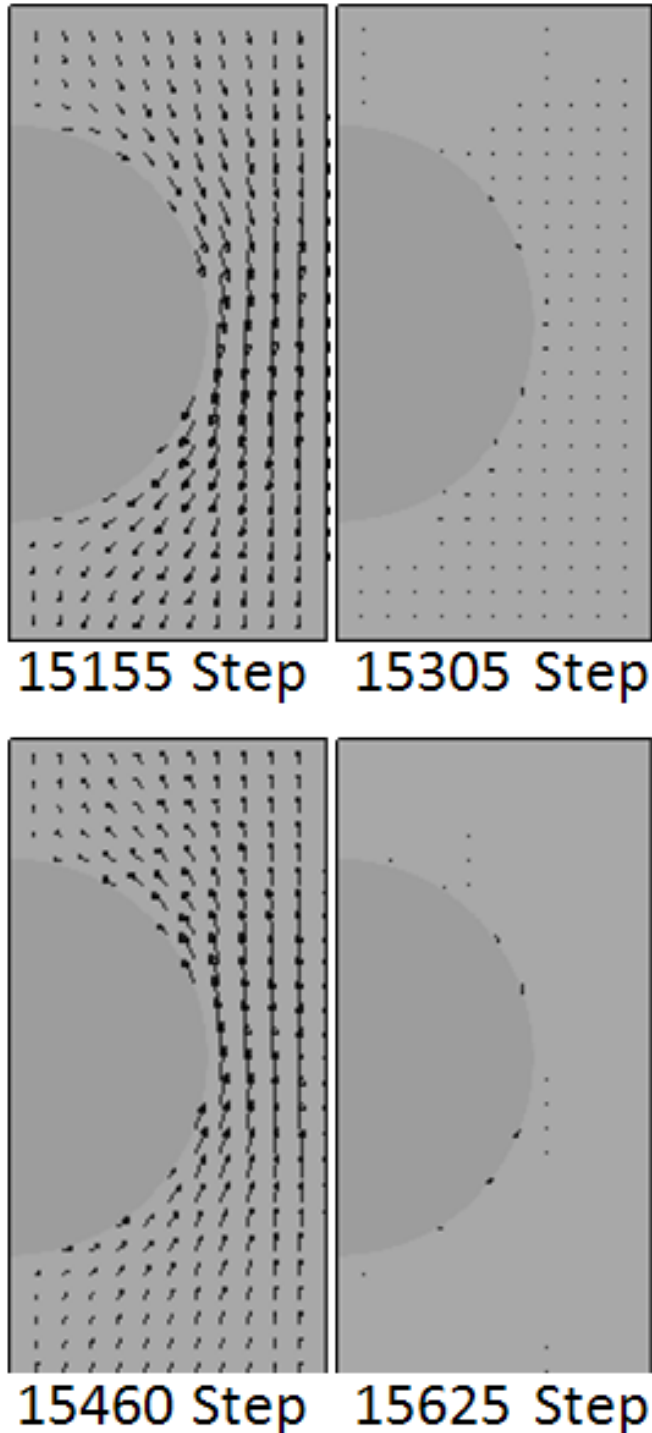


Fig. 8. Overall flow field around the droplet at later time.

clearly in Fig. 8.

The flow field at the side surface of the droplet at later time is shown in Fig. 9, corresponding to the early flow field in Fig. 6. The magnitude of the velocity vector inside the droplet is again 100 times larger than that outside the droplet as was the case in Fig. 6. It is found at 15155 time steps that the inside flow field is formed due to the outside downward flow field. At 15305 time

steps, the outside flow is upward near the droplet surface, while the outer flow far away from the droplet is still downward and very small. It is also shown in Fig. 8 that the outside flow field is almost zero at 15305 time steps. The outside flow field is clearly upward at 15460 time steps, and the inside flow field seems to be dragged by the outside flow field again. At 15625 time steps, the outside flow is downward near the droplet surface, while the outer flow away from the droplet is still upward and very small. This flow field is almost the reversed flow field of that at 15305 time steps. These oscillating flow fields at the side surface of the droplet are very similar to those in Fig. 6 for the early stage of the transient.

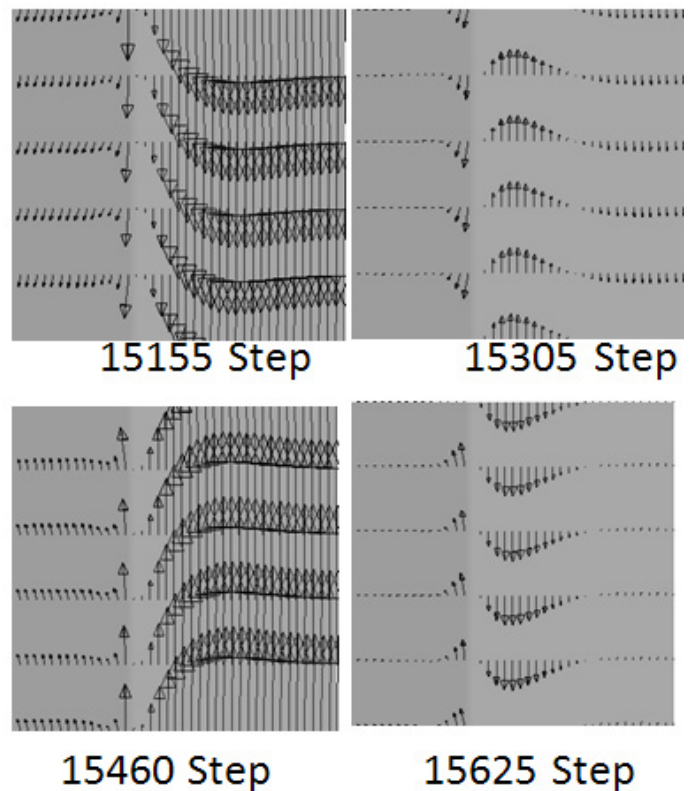


Fig. 9. Flow field at the side of the droplet at later time.

The flow field at the bottom surface of the droplet at later time is shown in Fig. 10, corresponding to the early flow field in Fig. 7. The magnitude of the velocity vector is the same between the inside and the outside of the droplet in Fig. 10. It is found at 15155 time steps that the outside flow is going from the right to the centre, and then downward. At 15305 time steps, the outside flow becomes smaller, but still seems to be

downward. Small rightward flows are, however, seen. In this time step, the recirculation flow region is larger than that in the early flow field shown in Fig. 7, and the upward flow is not clearly seen in this small region. The small rightward flow, however, becomes the upward flow at the side surface shown in Fig. 9. The downward flow is still seen at 15460 time steps. The rightward

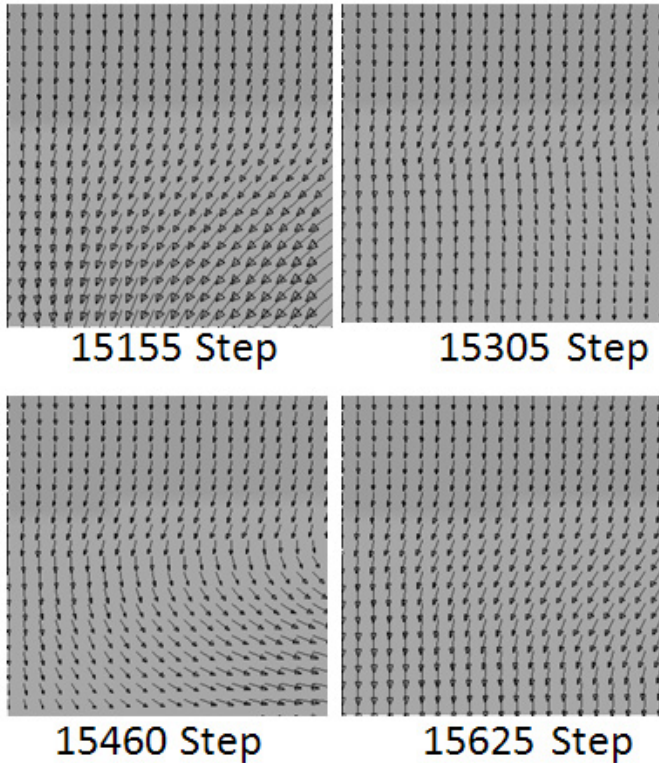


Fig.10. Flow field at the bottom of the droplet at later time.

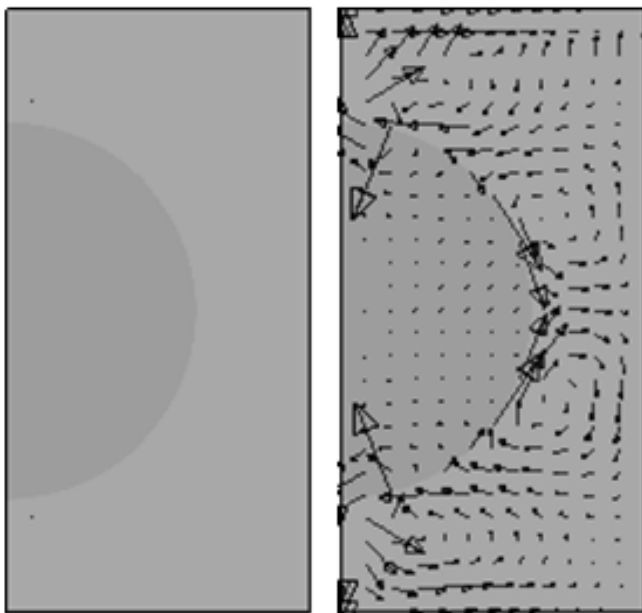


Fig. 11. Average flow field from 13750 to 14375 steps.

flow is, however, larger than at 15305 time steps. The overall flow is upward as shown in Fig. 8 at this time. It is thus found that the vortex region is large, and the vortex center is not included in this small region. The rightward flow shown in this region is going upward in the outside of the surface region. The downward flow is seen again at 15625 time steps, and the outside flow direction is from the right to the left. This leftward flow is coming from the side of the droplet as shown in Fig. 9. A similar flow region with upward flow also appears at the top of the droplet, though it is not shown here. It is found from the comparison of flow field between the early and later time steps that the vortex regions at the stagnation points on the droplet surface become larger in time.

E. Formation of Streaming Flows Field

Average flow field later time steps is shown in Fig. 11. The time average of the flow field is taken over one oscillation period from 13750 to 14375 time steps. The left part of Fig. 11 is using the same vector scale as used in Figs. 5 and 8. The average flow velocity is almost zero over one oscillation period, and thus no flow is seen. The right part of Fig. 11 is, however, using 200 times larger vector scale. It is found that the streaming flows appear in the average flow field, even though the velocity magnitude is still small. These streaming flows would become larger in time, and large scale direct current flows might be formed in the oscillating pressure field as the acoustic streaming flows seen in the experiments [5,6].

IV. CONCLUSION

In this study, the surface flows on a droplet in an oscillating pressure field have been simulated numerically by solving the Navier-Stokes equations using the arbitrary Lagrangian-Eulerian (ALE) and the level set coupled method. The pseudo-compressibility is assumed for the incompressible governing equations. The oscillating pressure variations as well as the oscillating flows were simulated well by the present numerical method. Detailed transient flow fields in and around the droplet were calculated by performing parallel computations with 256 processors, and the flow phenomena in a thin layer around the droplet surface were discussed.

The vortex or recirculation region was found to appear at the top and bottom stagnation points on the droplet surface. The oscillating flow was also shown in the thin layer along the droplet surface. This oscillating flow was formed by the recirculation flows at the top and bottom of the droplet. It was found that the phase of the oscillating flow in the thin layer was shifted from that in the outer layer away from the droplet. From the comparison of flow fields between the early and later time steps, the recirculation region was shown to grow in time. The recirculation flows and the flows in the thin layer would be the origin of the acoustic streaming flows observed in the ultrasonic levitator in the experiments. Our numerical approach for simulating gas-liquid interfaces using parallel computers would be applicable to simulations of complicated fluid phenomena involving two-phase interfaces [16] or free surfaces [17,18].

REFERENCES

- [1] I. Egry, G. Lohoefer, G. Jacobs, Surface tension of liquid metals: results from measurements on ground and in space, *Phys. Rev. Lett.* 75, 1995, 4043-4046.
- [2] V. Shatrov, V., Priede, J. and Gerbeth, G., Three-Dimensional Linear Stability Analysis of the Flow in a Liquid Spherical Droplet driven by an Alternating Magnetic Field, *Physics of Fluid*, 15,2003, 668-678.
- [3] Rhim, W.K. and Chung, S. K., Isolation of Crystallizing Droplets by Electrostatic Levitation, *Methods: A Companion to Methods in Enzymology*, 1, 1990, 118-127.
- [4] Yarin, A. L., Weiss, D. A., Brenn, G. and Rensink, D., Acoustically Levitated Drops: Drop Oscillation and Break-Up Driven by Ultrasound Modulation, *Journal of Multiphase Flow*, 28, 2002, 887-910
- [5] Trinh, E. H. and Robey, J. L., Experimental Study of Streaming Flows Associated with Ultrasonic Levitators, *Physics of Fluid*, 6,1994, 3567-3579.
- [6] Yarin, L. L., Brenn, G., Keller, J., Pfaffenlehner, M., Ryssel, E. and Tropea, C., Flowfield Characteristics of an Aerodynamic Acoustic Levitator, *Physics of Fluid*, 9, 1997, 3300-3314.
- [7] Rednikov, A. Y., Zhao, H., Sadhal, S. S. and Trinh, E. H., Steady Streaming Around a Spherical Drop Displaced from the Velocity Antinode in an Acoustic Levitation Field, *Journal of Acoustic Society of America*, 106, 1999, 3289-3295.
- [8] M. Sussman, P. Smereka, Axisymmetric free boundary problems, *J. Fluid Mech.* 341, 1997, 269-294.
- [9] Hirt, C. W., Amsden, A. A. and Cook, J. L., An arbitrary Lagrangian-Eulerian computing method for all flow speeds, *Journal of Computational Physics*, 14,1974, 227-253.
- [10] Y.C. Chang, T.Y. Hou, B. Merriman, S. Osher, A level set formulation of Eulerian interface capturing methods for incompressible fluid flows. *J. Comp. Phys.* 124, 1996, 449-464.
- [11] T. Watanabe, Parallel computations of droplet oscillations, *LNCSE*, 67, 2009, 163-170.
- [12] A.A. Amsden, F.H. Harlow, Simplified MAC technique for incompressible fluid flow calculations, *J. Comp. Phys.* 6, 1970, pp. 322-325.
- [13] T. Watanabe, Flow field and oscillation frequency of a rotating liquid droplet, *WSEAS Trans. Fluid Mech.*, vol. 3, 2008, pp. 164-174 .
- [14] M. Sussman, P. Smereka, S. Osher, A level set approach for computing solutions to incompressible two-phase flow, *J. Comp. Phys.* 114, 1994, pp. 146-159.
- [15] T. Watanabe, Nonlinear oscillations and rotations of a liquid droplet, *Int. J. Geology*, vol. 4, 2010, pp. 5-13 .
- [16] N. M. S. Hassan, M. M. K. Khan and M. G. Rasul, Characteristics of air bubble rising in low concentration polymer solutions, *WSEAS Trans. Fluid Mech.*, Vol. 2, 2007, pp. 53-60.
- [17] M. DeMarchis and E. Napoli, 3D Numerical simulation of curved open channel flows, *WSEAS Trans. Fluid Mech.*, Vol. 1, 2006, pp. 175-180.
- [18] L. A. Mironova, O. I. Gubanov and S. Kocabiyik, Numerical simulation of flow past an oscillating cylinder close to a free surface, *WSEAS Trans. Fluid Mech.*, Vol 1, 2006, pp. 297-303.

Tadashi Watanabe Ph. D. degree in Nuclear Engineering at Tokyo Institute of Technology, Japan, in 1985.

Research engineer in reactor safety division of Japan Atomic Energy Agency since 1985. The major research fields are nuclear reactor thermal hydraulics, reactor safety analysis, two-phase flow experiments and simulations, and computational science.

Member of Japan Atomic Energy Society, and Japan Mechanical Engineering Society.